ELSEVIER

Contents lists available at ScienceDirect

Ultrasonics

journal homepage: www.elsevier.com/locate/ultras





Exploiting nonlinear wave propagation to improve the precision of ultrasonic flow meters

Jack Massaad ^{a,*}, Paul L.M.J. van Neer ^{a,c}, Douwe M. van Willigen ^b, Nicolaas de Jong ^{a,d}, Michiel A.P. Pertijs ^b, Martin D. Verweij ^{a,d}

- a Delft University of Technology, Department of Imaging Physics, Laboratory of Medical Imaging, Lorentzweg 1, 2628CJ, Delft, The Netherlands
- b Delft University of Technology, Department of Microelectronics, Electronic Instrumentation Laboratory, Mekelweg 4, 2628CD, Delft, The Netherlands
- c TNO, Department of Acoustics and Sonar, Oude Waalsdorperweg 63, 2597AK, The Hague, The Netherlands
- d Erasmus MC, Thorax Center, Department of Biomedical Engineering, Doctor Molewaterplein 40, 3015GD, Rotterdam, The Netherlands

ARTICLE INFO

Keywords: Ultrasonic flow meter KZK equation Nonlinear acoustics

ABSTRACT

Acoustic wave propagation in ultrasonic flow measurements is typically assumed to be linear and reciprocal. However, if the transmitting transducer generates a sufficiently high pressure, nonlinear wave propagation effects become significant. In flow measurements, this would translate into more information to estimate the flow and therefore a higher precision relative to the linear case. In this work, we investigate how the generated harmonics can be used to measure flow. Measurements in a custom-made flow loop and simulations using the Khokhlov-Zabolotskaya-Kuznetsov (KZK) equation will show that the second harmonic component provides similar transit time differences to those obtained from the fundamental component, their linear combination results in more precise flow measurements compared to the estimations with the fundamental component alone.

1. Introduction

Ultrasound is a common modality to measure flow in an industrial setting [1-5]. There are two types of ultrasonic flow sensors: in-line sensors and clamp-on sensors. The first configuration usually consists of a perforated pipe section with aligned pairs of transducers in direct contact with the flow (Fig. 1a), and the second configuration typically consists of a pair of single element transducers that are fixed on the outside of the pipe wall (Fig. 1b). In either configuration, the propagation direction of the acoustic waves generated by the transducers has a component parallel to the pipe axis, which makes the travel time of the waves sensitive to the flow [6]. As a result, the acoustic wave with a propagation component in the direction of the flow (downstream) travels faster than the one that propagates with a propagation component in the opposite direction of the flow (upstream). The ultrasonic flow meter system (including acoustic waves, transducers, and electronics) is assumed to be reciprocal, which means that, in the absence of flow, the system response remains unchanged when the role of transducers A and B are interchanged [7]. Moreover, linear flow theory is assumed, i.e. the transit time difference or phase difference between upstream and downstream waves is directly proportional to the flow speed [8].

Provided that both upstream and downstream time pulses $s_{\rm u}(t)$ and $s_{\rm d}(t)$ have the same shape but show a relative time difference, their

cross-correlation will have a peak at a time instant that corresponds to the delay between both signals [9]. The cross-correlation algorithm is often implemented to measure flow speed [10–13] because it has a low sensitivity to the random (thermal) noise occurring in the flow, the electrical components, and the transducers in typical ultrasonic flow meter systems [3,13].

However, the precision of cross-correlation algorithms in estimating transit time differences is limited by factors such as the total available bandwidth of the system, and the length and signal-to-noise ratio (SNR) of the applied time pulses [14]. In practice, the bandwidth of the system cannot be increased since it depends on the properties of the installed transducers. Also, the frequency dependent amplitude behavior of the system causes challenges in generating long coded excitations that perform favorable with cross-correlation algorithms, e.g. chirps.

It is often implicitly assumed that during ultrasonic flow measurements acoustic wave propagation is linear (this should not to be confused with linearity of the flow speed metering). However, it is well known from the acoustic literature that wave propagation is actually a nonlinear phenomenon [15]. At sufficiently high pressures, nonlinear wave propagation effects become significant and the resulting harmonics may be recorded when these fall within the bandwidth of the system. In practice, from each recorded time signal two versions can be

E-mail address: J.M.MassaadMouawad@tudelft.nl (J. Massaad).

^{*} Corresponding author.

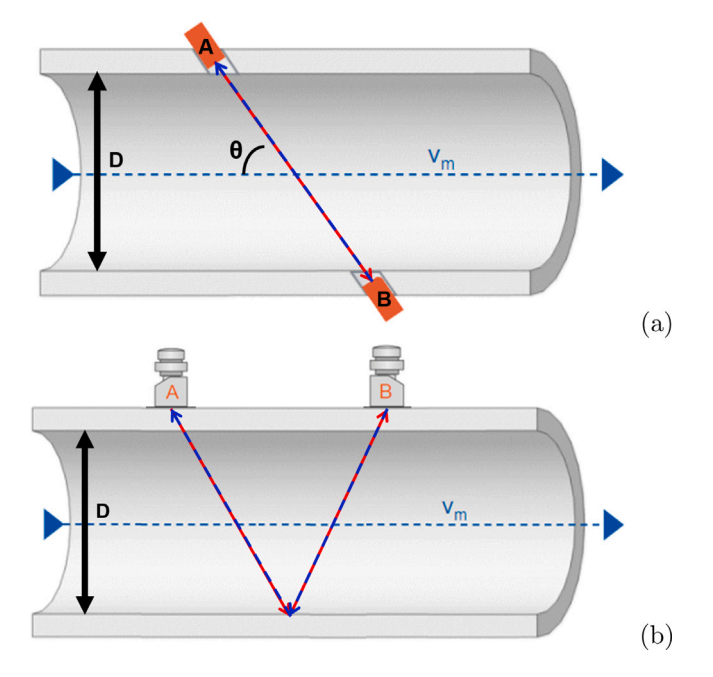


Fig. 1. Ultrasonic (a) in-line and (b) clamp-on flow meter configuration. A liquid moves from left to right with a flow speed v_m within a pipe with an inner diameter D. The solid red and dashed blue arrows indicate the downstream and upstream travel paths of the acoustic beams generated by transducers A and B, respectively. Modified from [16].

extracted by filtering: one with a frequency band centered around the fundamental (transmitted) frequency, and another one with a frequency band centered around the second harmonic (twice the transmitted) frequency. To the best of the authors' knowledge, the extra frequency band generated by nonlinear wave propagation is not used in current ultrasonic flow meter designs.

In this paper, we will show that in a realistic flow metering system a higher pressure in the fundamental frequency band will lead to nonlinear wave propagation. Furthermore, we also test the hypotheses that the second harmonic frequency band may also be used to estimate the flow speed, and that this increases the total number of flow estimates, which improves flow measurement precision. Also, we will discuss some challenges that are imposed by applying nonlinear wave propagation.

The paper is structured as follows. Section 2 describes the theory and the parameters used to simulate nonlinear wave propagation in an ultrasonic flow metering scenario. Section 3 describes and discusses experiments done to measure flow speeds of water up to $0.5\,\mathrm{m/s}$ in a system showing nonlinear wave propagation. The measurement scenario has been simulated for flow speeds up to $200\,\mathrm{m/s}$, and the obtained results are shown and discussed in Section 4. The practical usefulness of the method is discussed in Section 5. Finally, main conclusions are summarized in Section 6.

2. Theory

In this section, linear ultrasonic flow metering theory is presented. Moreover, the KZK equation for modeling nonlinear acoustic wave propagation is described. In ultrasonic flow metering, acoustic waves propagate under an angle relative to the flow direction (see Fig. 1). In contrast, the KZK equation provides the acoustic wavefield parallel to the propagation axis of the wave. Therefore, the assumptions and approximations that make it possible to use the KZK equation to model nonlinear wave propagation in an ultrasonic flow metering scenario are also presented.

2.1. Linear ultrasonic flow metering

A typical configuration of a flow metering system is shown in Fig. 1a. Two single-element transducers, in direct contact with the flow and facing each other under a certain angle θ relative to the direction of the flow, i.e. the pipe axis, are excited [17,18] and the transit time of the respective upstream (t_u) and downstream (t_d) acoustic waves is given by [8]:

$$t_{u} = \frac{D}{\sin \theta} \frac{1}{c_{0} - v_{m} \cos \theta},$$

$$t_{d} = \frac{D}{\sin \theta} \frac{1}{c_{0} + v_{m} \cos \theta},$$
(1)

where D represents the inner diameter of the pipe, c_0 represents the small-signal sound speed of the fluid, and v_m represents the flow speed. Combining the expressions of Eq. (1), a linear relation between the flow speed, and the transit time difference Δt is obtained:

$$v_m = \frac{D}{\sin 2\theta} \frac{t_u - t_d}{t_u t_d} \approx \frac{c_0^2 \tan \theta \, \Delta t}{2D}.$$
 (2)

In the last step a quadratic term in v_m has been neglected because it can be assumed that $v_m \ll c_0$ (see Appendix).

2.2. Nonlinear acoustic wave propagation

Diffraction, absorption and nonlinearity effects of a beam-like wave generated by a transducer can be simulated using the parabolic approximation of the wave equation provided by the Khokhlov–Zabolotskaya–Kuznetsov (KZK) equation. In Cartesian coordinates, the 3D-KZK equation can be expressed as:

$$\frac{\partial p}{\partial z} = \frac{c_0}{2} \int_{-\infty}^{t'} \left(\frac{\partial^2 p}{\partial x^2} + \frac{\partial^2 p}{\partial y^2} \right) dt'' + \frac{\delta}{2c_0^3} \frac{\partial^2 p}{\partial t'^2} + \frac{\beta}{2\rho_0 c_0^3} \frac{\partial p^2}{\partial t'}. \tag{3}$$

In Eq. (3), p=p(x,y,z,t') represents the acoustic pressure in the medium, z the axial coordinate (perpendicular to the transducer surface), x and y the lateral coordinates (parallel to the transducer surface), $t'=t-\frac{z}{c_0}$ the retarded time with t begin the actual time, δ the diffusivity of sound of the medium, ρ_0 the density of mass of the medium, and β the coefficient of nonlinearity of the medium, defined as:

$$\beta = 1 + \frac{B}{2A},\tag{4}$$

where B/A is known as the parameter of nonlinearity.

Different methods to solve Eq. (3) have been proposed [19–23]. Usually, a transformation of Eq. (3) is performed [22]:

$$P = p/p_0$$
, $\chi = x/r$, $\psi = y/r$, $\sigma = z/d$, $\tau = \omega_0 t'$, (5)

where p_0 is the maximum pressure at the surface of the transducer, d is the characteristic range length (for which we have taken d=1 m), r is the characteristic transverse length (for which we have taken the transducer aperture), and ω_0 is the central angular frequency of the transmitted pressure pulse. Substituting the expressions of Eq. (5) into Eq. (3) yields:

$$\frac{\partial P}{\partial \sigma} = \frac{1}{4G} \int_{-\infty}^{\tau} \left(\frac{\partial^2 P}{\partial \chi^2} + \frac{\partial^2 P}{\partial \psi^2} \right) d\tau' + A \frac{\partial^2 P}{\partial \tau^2} + N P \frac{\partial P}{\partial \tau}, \tag{6}$$

where the dimensionless coefficients G, A and N follow as:

$$G = z_0/d, \quad A = \alpha_0 d, \quad N = d/\bar{z}, \tag{7}$$

where $z_0=\omega_0 r^2/2c_0$ represents the Rayleigh distance, $\alpha_0=\delta\omega_0^2/2c_0^3$ is the attenuation coefficient of the medium and $\bar{z}=\rho_0c_0^3/\beta\omega_0\rho_0$ is the plane wave shock formation distance. The first term at the right-hand side of Eq. (6) accounts for diffraction, the second term for absorption, and the third term for nonlinear behavior of the acoustic wave.

Here, the time-domain numerical approach developed by [22] to solve Eq. (6) was implemented.

2.2.1. Modeling assumptions and approximations

The propagation speed of a progressive nonlinear wave, propagating in the z-direction in a medium without flow is given by [15] as:

$$\frac{dz}{dt} = c_0 + \beta u,\tag{8}$$

where u is the particle velocity, i.e. the velocity of the medium due to the acoustic wave. Substituting Eq. (4) into Eq. (8), we get:

$$\frac{dz}{dt} = c_0 + \left(1 + \frac{B}{2A}\right)u = \left(c_0 + \frac{B}{2A}u\right) + u. \tag{9}$$

As reported in [15], assuming an isentropic (i.e. adiabatic) fluid, the term in parenthesis at the right-hand side of Eq. (9) is the large-signal sound speed of the medium, c, so:

$$\frac{dz}{dt} = c + u. ag{10}$$

Here we see that the propagation speed of the nonlinear wave is the sum of the large-signal sound speed and the motion of the medium induced by the acoustic wave. The latter can be compared to the 'wind effect' in outdoor sound propagation. In this work, we assume that the flow speed v_m adds linearly to the 'wind effect' term, so the total propagation speed of the wave is given by:

$$\frac{dz}{dt} = c + u + v_m \cos \theta = (c_0 + v_m \cos \theta) + \beta u, \tag{11}$$

where θ represents the angle of propagation of the acoustic beam relative to the direction of the flow (i.e. the pipe axis). Comparison of Eqs. (8) and (11) shows that the flow of the medium can be accounted for by adding a correction term to the small-signal sound speed of the medium.

2.2.2. Simulation settings

The following medium parameters were considered for the simulation of nonlinear wave propagation in water: $\rho_0=1000\,\mathrm{kg/m^3}$, $\alpha_0=0.002\,\mathrm{dB/MHz.cm}$, and $\beta=3.5$. To account for the flow of the medium, the small-signal wave speed of the medium was taken to be:

$$c_0' = 1500 \,\mathrm{m/s} \mp v_m \cos \theta, \tag{12}$$

with $\theta=45^{\circ}$ being the angle of the transducer axis relative to the flow direction. Furthermore, upstream and downstream wave propagation was considered by either taking the – or the + sign, respectively, in Eq. (12).

As source signature, a 5-cycle Gaussian-modulated sine wave, with a center frequency of $f_0=2.3\,\mathrm{MHz}$, was used. Moreover, a spatial discretization of $\Delta\sigma=0.06$ (equivalent to ≈ 10 points per wavelength) was defined and found to be sufficient to discard potential numerical dispersion effects in the solution of the KZK equation.

Considering a rectangular transducer aperture, the range of validity of the implemented solution of the KZK equation was reported in [24]:

$$z > \sqrt{\frac{a^2 + b^2}{2}} \left(k \sqrt{\frac{a^2 + b^2}{2}} \right)^{1/3},$$
 (13)

where 2a and 2b are the dimensions of the rectangular aperture, and k represents the wavenumber. Here we have chosen a transducer aperture of $12 \,\mathrm{mmx} 16 \,\mathrm{mm}$, which is equal to our design of a transducer for generating nonlinear waves in an ultrasonic flow meter. In this case, the range of validity of the KZK equation starts at a depth of $z > 29.8 \,\mathrm{mm}$. For a pipe with an inner diameter of $D = 40 \,\mathrm{mm}$, the implementation of [22] for solving the KZK equation is valid for simulating the ultrasonic flow measurement in the setting of Fig. 2.

3. Experimental study

3.1. Flow setup

A custom-made flow loop was built and filled with water (Fig. 2). Moreover, a custom flow sensor was built. It consisted of two single-element transducers (V382, Olympus, Tokyo, JP) with a diameter of



Fig. 2. Our custom-made flow loop for ultrasonic flow measurements. The custom-made flow sensor is installed in an acrylic pipe with an inner diameter of 40 mm. Flow moves through the sensor from left to right.

12.7 mm, a center frequency of $f_c=3.5\,\mathrm{MHz}$, and a $-6\,\mathrm{dB}$ bandwidth between $2.24-4.42\,\mathrm{MHz}$. The transducers were placed 45° relative to the axis of a pipe with an inner diameter of $D=40\,\mathrm{mm}$. Furthermore, a gear pump was used to hold-off air bubbles within the loop during flow measurements, because bubbles would have an adverse scattering effect on the ultrasound waves. With this configuration, it was possible to achieve flow speeds up to $v_m=0.5\,\mathrm{m/s}$. Flow speed was also measured by a reference ultrasonic flow meter (Optosonic 3400, KROHNE Nederland B.V., Dordrecht, NL).

3.2. Data acquisition

A 5-cycle Gaussian-modulated sine wave with a center frequency of $f_c=2.3\,\mathrm{MHz}$ and a peak-to-peak voltage of $0.6\,\mathrm{V}$ was generated using an arbitrary waveform generator (AWG; Agilent 33521 A, Keysight Technologies, Santa Rosa, CA, USA), and amplified by a $50\,\mathrm{dB}$ amplifier (2100L RF Amplifier, Electronic Navigation Industries, Rochester, NY, USA), to achieve a signal with a peak-to-peak voltage of $180\,\mathrm{V}$. For larger voltages, nonlinearities of the electronic equipment were no longer negligible. The amplified signal was directed to a custom printed circuit board (PCB) that was built to perform a fast $50\,\mathrm{ms}$ switching between upstream and downstream flow measurements. The same amplified signal was also directed to an attenuator (Bench Top Attenuator, JFW Industries Inc., IN, USA) and then recorded simultaneously with the received signal by an acquisition card (M3i.4142 Spectrum Instrumentation GMbH, Großhansdorf, DE).

Five flow speeds were measured, and 1000 upstream and downstream signal pairs were recorded for each considered speed.

3.3. Signal processing

A flowchart of the signal processing algorithm developed to extract transit time differences is shown in Fig. 3, which includes the filtering of the bandwidth around the fundamental ($f_1 = 2.3\,\mathrm{MHz}$) and second harmonic ($f_2 = 4.6\,\mathrm{MHz}$) of the recorded signals. This processing scheme was implemented on the 1000 upstream–downstream signal pairs recorded for each flow speed. Finally, an average transit time difference was estimated from the fundamental frequency band (1000 Δt_{f1} values), the second harmonic frequency band (1000 Δt_{f2} values), and the combined fundamental and second harmonic bands (1000 Δt_{f1} and 1000 Δt_{f2} , i.e. 2000 values).

3.4. Results and discussion

A typical measured signal is shown in Fig. 4a. Furthermore, the magnitude of its Fast Fourier Transform (FFT) in Fig. 4b clearly shows a second harmonic component centered at 4.6 MHz generated by nonlinear wave propagation, with an amplitude approximately 24 dB below that of the fundamental component. If the fundamental frequency is

J. Massaad et al. Ultrasonics 116 (2021) 106476

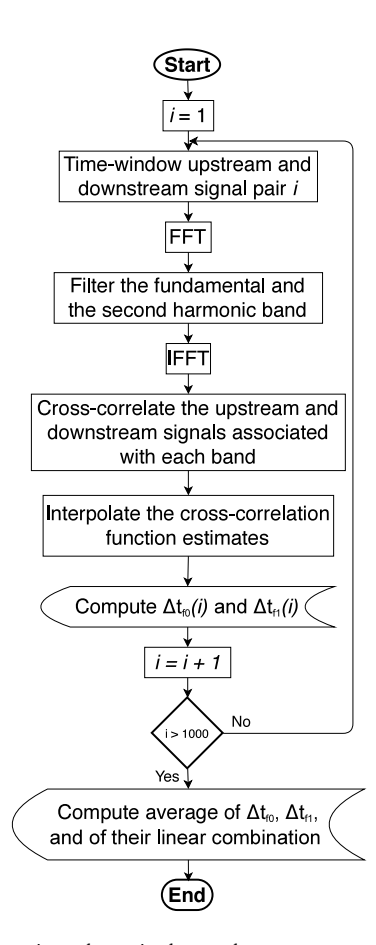


Fig. 3. Signal processing scheme implemented to extract transit time difference from the 1000 upstream–downstream measured time signal pairs recorded for each considered flow speed.

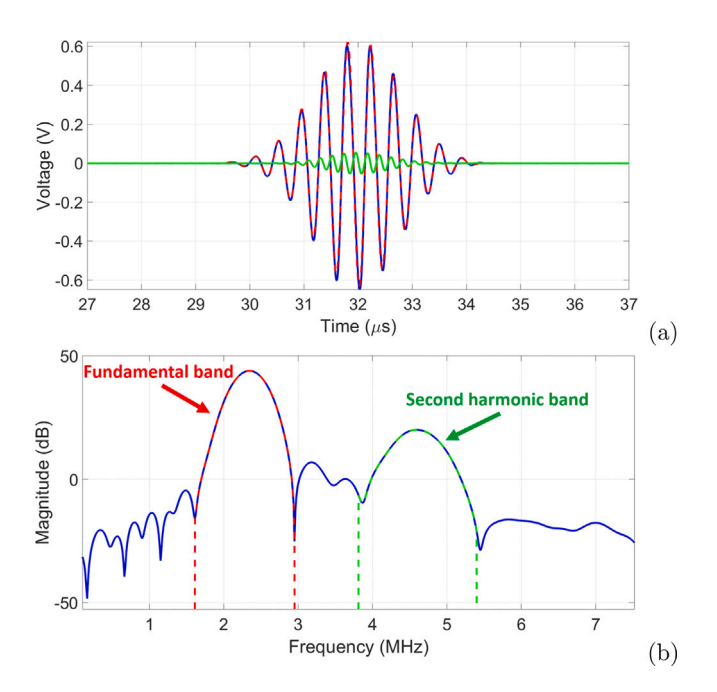


Fig. 4. (a) A measured nonlinear time signal during flow measurements (blue), as well as its fundamental (red) and second harmonic (green) components. (b) Magnitude of the Fast Fourier Transform (FFT) applied on the time signal shown in (a).

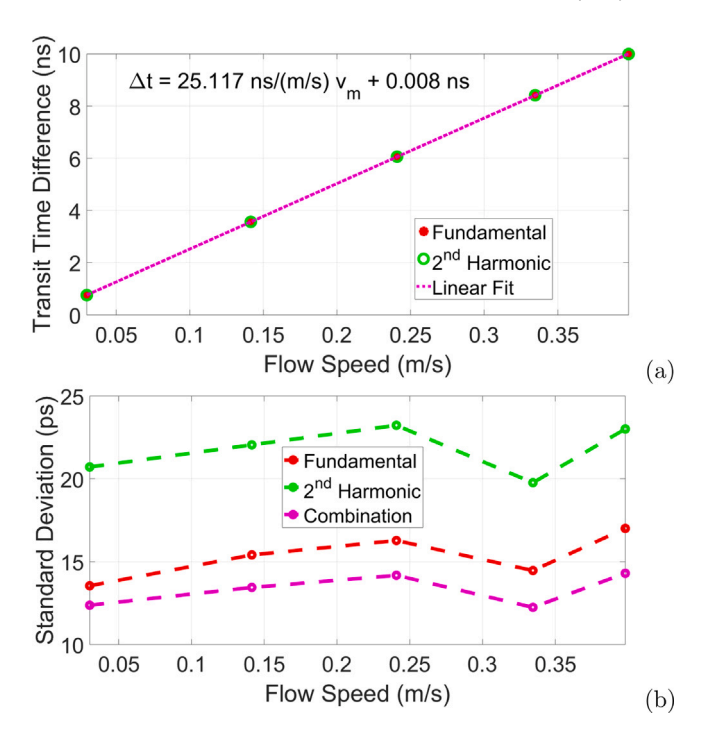


Fig. 5. (a) Measured linear relation between transit time difference and flow speed, for both the fundamental and the second harmonic of the time signals. (b) Standard deviations of the computed transit time differences for the fundamental, the second harmonic, and their combination.

chosen in the lower part of the frequency band of the transducer, the second harmonic frequency could be recorded in the upper part of the frequency band of the same transducer. This approach has been followed for our measurements.

For upstream and downstream time signals related to the second harmonic, the only non-reciprocal factor was the flow speed. Thus, regardless of their difference in amplitude and in transit time of the second harmonic components relative to the unfiltered time signals, it was expected for their relative transit time difference (Δt_{f2}) to be similar to that associated with the fundamental components (Δt_{f1}). This approach has been followed for our measurements. Results in Fig. 5a show that the transit time differences computed from the second harmonic are indeed similar to those of the fundamental. Therefore, when both estimates are used, the standard deviation of the flow estimate becomes lower than the one obtained using only the fundamental or the second harmonic, as confirmed by Fig. 5b. The linear fit on the measured data reported a coefficient of determination of $R^2 = 0.9999$.

In ultrasonic flow metering of high flow speeds, i.e. when v_m is comparable to c, the upstream and downstream effective wave speeds are different, as seen from Eq. (11). Therefore, it is expected that each signal would distort differently relative to the other. Moreover, the quadratic term discarded in Eq. (2) may no longer be omitted (see Appendix), and the transit time difference estimations would not follow the expected linear trend with flow speed observed in Fig. 5a. Since it was not possible to achieve higher flow speeds in our flow loop, nonlinear wave propagation simulations were performed to cross-check the linear results of Fig. 5a, and to study the effect of very high flow speeds on transit time difference estimations.

4. Simulation study

In the simulations, the parameter p_0 had to be chosen properly to achieve a good correspondence between the measured and simulated pressures. The value of this parameter was determined by comparing the magnitude of the FFT of a measured time signal with that of a

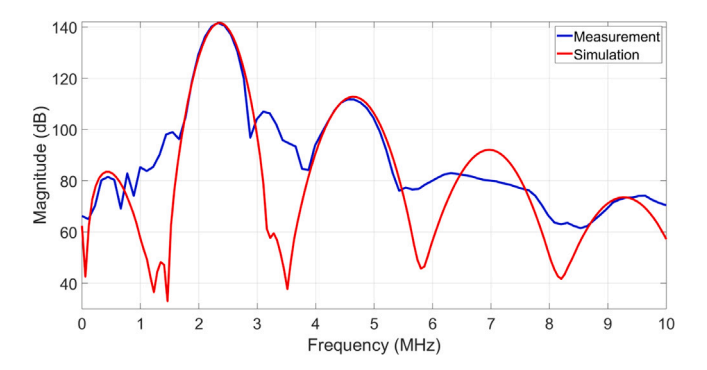


Fig. 6. Magnitude of the FFT performed on received signals for the measured (blue) and simulated (red) waveforms, for the simulation parameter $p_0 = 0.2\,\mathrm{MPa}$ that gives the best overlap.

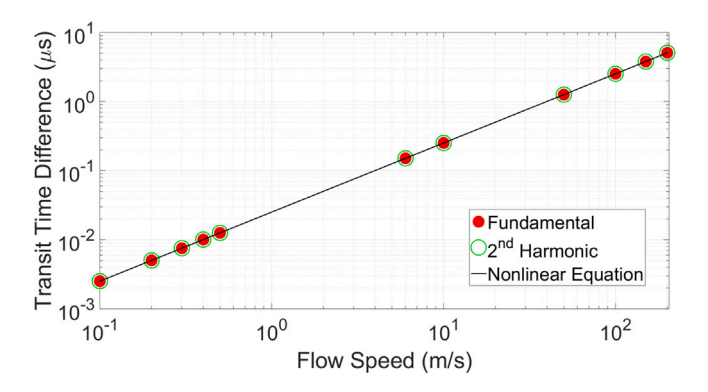


Fig. 7. Simulation results of transit time difference as a function of flow speed, as obtained from the fundamental (dots) and the second harmonic (circles). The black line represents the theoretical nonlinear relation between both quantities, given by Eq. (A.7).

simulated one. The best possible overlap of both spectra was achieved with a value of $p_0=0.2\,\mathrm{MPa}$ (Fig. 6).

Using this value and the previously defined simulation parameters, low and high flow speed scenarios were simulated. In view of the considered pipe diameter and the flow speeds able to be reached with our flow loop, values of $v_m > 0.5 \, \text{m/s}$ were labeled as high flow speeds.

4.1. Low flow speeds

Five flow speeds between $v_m = 0.1 \, \text{m/s}$ and $v_m = 0.5 \, \text{m/s}$ were considered, which covers the range of the measurements in Fig. 5a. After applying the same signal processing scheme as for the measurements, similar results were obtained (see Fig. 7). The transit time differences estimated using cross-correlation, and the flow speeds computed via Eq. (A.7) reported deviations (relative errors) from the theoretically expected values of less than 0.04% (see Fig. 8).

4.2. High flow speeds

When the flow speed is of the same order of magnitude as the small-signal sound speed, it is be expected from Eq. (12) that the upstream and downstream waves will undergo a different amount of nonlinear deformation. The question would then be whether Eq. (A.7) still holds for the fundamental and the second harmonic. To simulate this scenario, flow speeds of 6 m/s, $10 \, \text{m/s}$, $50 \, \text{m/s}$, $100 \, \text{m/s}$, $150 \, \text{m/s}$ and $200 \, \text{m/s}$ were considered.

Similarly to the scenario of low flow speeds, the transit time differences estimated via cross-correlation and the computed flow speeds using Eq. (A.7) reported comparable deviations, which were also below 0.04% (see Fig. 8). Due to the nonlinear relation between Δt and v_m ,

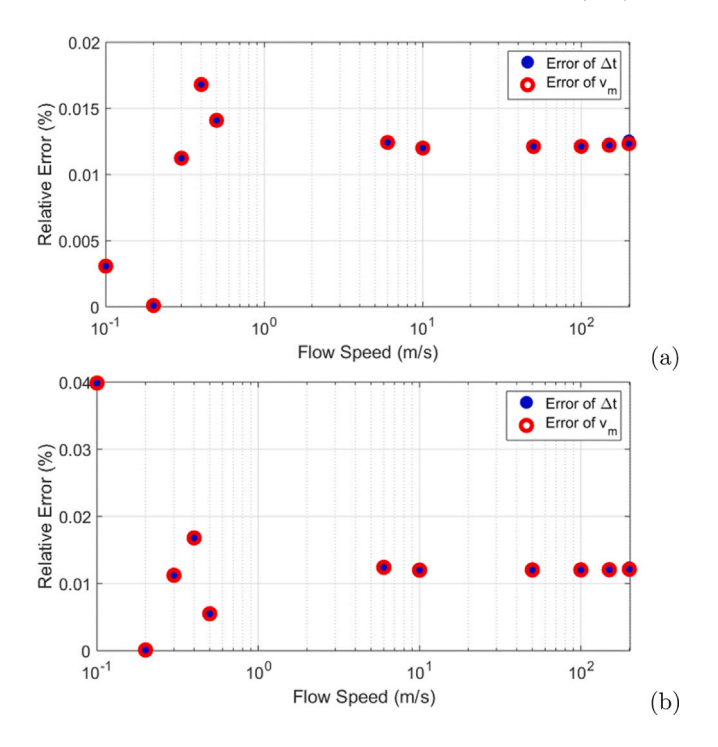


Fig. 8. Relative error between theoretically expected values and those extracted from (a) the fundamental and (b) the second harmonic band of the time signals obtained from KZK simulations. Blue bullet points and red circles represent the errors of the transit time difference and the flow speed, respectively.

the error in the flow speed for the highest considered value (i.e. $v_m = 200\,\mathrm{m/s}$) is slightly lower than the error in the transit time difference.

Furthermore, it was also observed that for increasing flow speed, the nonlinear distortion increases for the upstream wave and decreases for the downstream wave (see Fig. 9, particularly the increase (decrease) in the magnitude of the Fourier spectra associated to the upstream (downstream) time signals obtained when considering $v_m = 200\,\mathrm{m/s}$, relative to their spectra when considering low flow speeds). We thus see that this effect is non-reciprocal for upstream and downstream signals.

4.3. The effect of nonlinear wave propagation

Already from Fig. 8 it may be interpreted that the nonlinearity due to wave propagation has an insignificant contribution in the discrepancy of Δt and v_m with the ground truth. Nevertheless, we performed KZK simulations considering the same range of flow speeds, an initial pressure of $p_0=0.2\,\mathrm{kPa}$ (i.e. 1000x smaller than in previous simulations), and did not consider the nonlinear term of Eq. (3). As expected, the obtained errors in Δt and v_m were comparable to those shown in Fig. 8a.

5. Discussion

Nonlinear wave propagation applied to ultrasonic flow measurements is beneficial because the second harmonic upstream and downstream signals provide additional flow speed estimations that can increase the precision of the measurement. However, nonlinear propagation is non-reciprocal for upstream and downstream waves at nonzero flow because these experience a different wave speed. This becomes manifest when the flow speed cannot be considered small relative to the small-signal sound speed. Moreover, for these higher flow speeds linear flow theory, i.e. the linear relation between transit time difference Δt and flow speed v_m given in Eq. (2), no longer holds.

Next, we further elaborate on the limitations of the method presented in this paper, and also discuss how it could be implemented in practice.

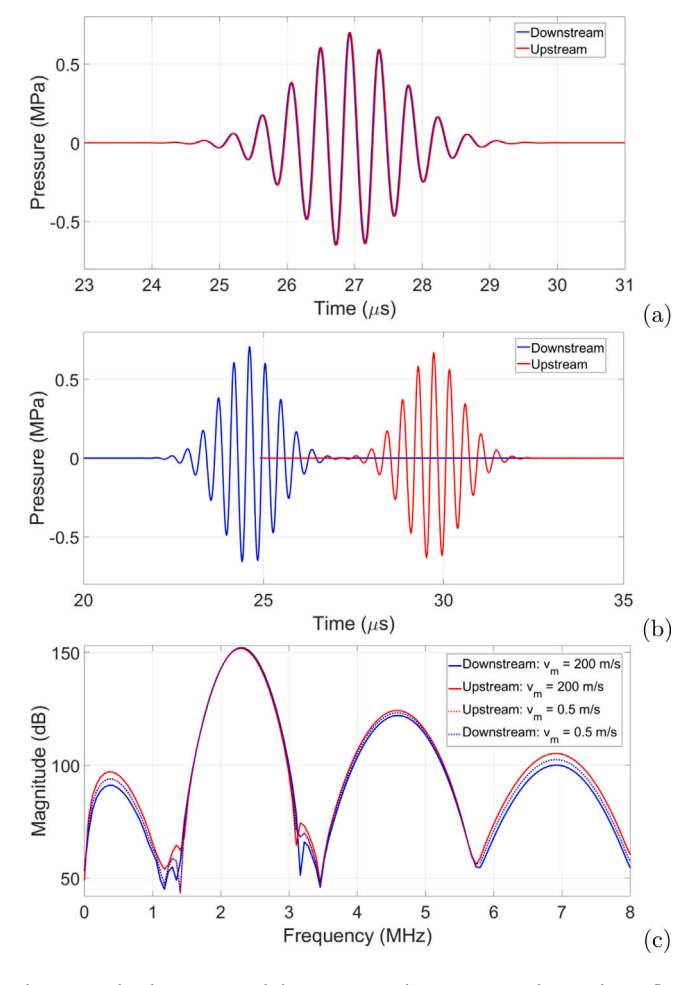


Fig. 9. Simulated upstream and downstream nonlinear time signals considering flow speeds of (a) $v_m=0.5\,\mathrm{m/s}$ and (b) $v_m=200\,\mathrm{m/s}$. (c) Magnitude of the Fourier spectra of the signals shown in (a) and (b).

5.1. Transit time difference between non-reciprocally distorted signals

Cross-correlating two signals, e.g. an upstream and a downstream flow measurement, to estimate their transit time difference is usually performed under the assumption that the correct arrival time difference is obtained, provided both signals have the same shape. This is not generally true, though, as may be demonstrated by the case of nonlinear wave propagation.

In a practical situation, the recorded signals will always show a reciprocal time shift between the fundamental and the second harmonic. This will be caused by the frequency dependent phase behavior of the receiving transducer and the electronics. Using the whole received waveform (i.e. the one that contains both the fundamental and the second harmonic bandwidth) in a cross-correlation approach will in theory make the transit time difference between upstream and downstream signals dependent on this time shift. This unwanted dependence is caused by the cross-correlation between the downstream fundamental and the upstream second harmonic, as well as the crosscorrelation between the upstream fundamental and the downstream second harmonic. The effect causes an error in the transit time difference. However, if we perform the cross-correlation between the separate downstream and upstream fundamental or the separate downstream and upstream second harmonic, the time shift between fundamental and second harmonic will not play a role, and both correlation results will show the exact transit time difference between upstream and downstream signals.

As we observed from our measurements, the amplitudes associated to the second harmonic are about 16 times smaller than the amplitudes associated to the fundamental (see Fig. 4a). On the one hand, this makes that by keeping the fundamental and second harmonic together, the above error was not noticeable even for high flow speeds ($v_m = 200\,\mathrm{m/s}$) for which the waveform distortion is different for upstream and downstream signals. On the other hand, we also did not see that the larger spectrum yields a better result. In fact, the reported flow speed values were very similar to those reported for the fundamental bandwidth.

5.2. SNR and standard deviation

In most acoustic flow measurement systems, the signal-to-noise ratio (SNR) is limited by the thermal noise of the transducers and the electronic components. Because the fundamental and second harmonic frequency bands do not overlap, the noise in these frequency bands can be considered as being uncorrelated. Moreover, the transit time difference between upstream and downstream fundamental signals is the same as the transit time difference between the second harmonic signals. This also holds when there is a reciprocal time shift between the fundamental and second harmonic signals. The foregoing implies that separation of the fundamental and the second harmonic signals effectively doubles the amount of data, and although the second harmonic signal has a lower SNR than the fundamental signal, adding the second harmonic data will improve the measurement precision, as demonstrated in this paper. Because of the lower SNR of the second harmonic, the precision will not increase by $\sqrt{2}$, and it is still up for debate how much precision is gained by addition of measurement points derived from the second harmonic. To answer this question, the trade-off between the SNR of the fundamental and that of the second harmonic should be investigated in more detail to further delineate the conditions under which useful flow measurements may be performed with separate consideration of the second harmonic.

At high flow speed conditions, the flow-related noise also becomes significant, which ultimately reduces the SNR of the received signal and thus, limits the usefulness of the second harmonic. Moreover, the flow may partially or entirely "wash-up" the beam and also modify its trajectory during propagation, making it difficult to measure it or even identify it upon reception.

Given that the standard deviation of an acoustic measurement is proportional to the available system bandwidth and the length of the pulse [25], it could be argued that, instead of using the fundamental and second harmonic in a system with nonlinear wave propagation, spikes or chirps could be used in a linear system to achieve the same standard deviation. However, the inherently limited bandwidth of ultrasound transducers and a further bandwidth reduction caused by the frequency content of the flow noise and the attenuation of the medium [26], make it challenging to achieve broadband input signals such as spikes (e.g. a Dirac δ pulse) or chirps in practice. Also, it becomes challenging to produce a chirp with practical amplifiers that always show some degree of nonlinear behavior and a frequency-dependent amplification factor. Furthermore, for such amplifiers the complexity, and therefore the cost, is proportional to the bandwidth.

5.3. Practical implementation

Generally, there is a high difference between the acoustic impedance of the transducer and the flowing medium, especially in a gas flow metering setting [27]. Therefore, the main practical measure being taken to achieve the required SNRs, is to increase the input voltage on the transducers [28]. By doing so, the amplitude of the fundamental could increase to such a level that a second harmonic is generated due to nonlinear wave propagation. As a consequence, more information is retrieved with the same transducers, provided these have sufficient bandwidth to record both the fundamental and the second

J. Massaad et al. Ultrasonics 116 (2021) 106476

harmonic. It is also important to mention that, in contrast to liquid flow, practical flow speeds achieved during gas flow metering may reach values in the same order of magnitude as the sound speed and, thus, upstream and downstream signals may deform very differently.

Ultrasonic flow meters are designed for the most attenuating liquid/gas that can be expected in the pipeline. Therefore, in less extreme situations, the electric system of the sensor is actually overdimensioned and, within the typical safety limits, is able to provide increased amplitudes of the fundamental that will induce significant nonlinear wave propagation. Hence, in practice it seems feasible and beneficial to use nonlinear wave propagation to extract more information from the measurements and thus achieve more precise flow estimates than with the fundamental signal alone.

Finally, even though the idea presented here has been implemented with in-line flow meters, considering the same assumptions, it could be implemented in clamp-on flow meters as well.

6. Conclusion

In this paper, we have introduced a method to employ nonlinear wave propagation for measuring flow speed in liquids. Using nonlinear wave propagation, the number of flow estimates per measurement, and thus the measurement precision, can be increased. At low flow speeds, good agreement was obtained between measurements and simulations. At high flow speeds, the simulations showed a deviation from the linear relation between the transit time difference and the flow speed, which was caused by the nonreciprocal behavior of the upstream and downstream nonlinear waves.

Declaration of competing interest

The authors declare that they have no known competing financial interests or personal relationships that could have appeared to influence the work reported in this paper.

Acknowledgments

This work is part of the research programme FLOW+, which is financed by the Dutch Technology Foundation STW, The Netherlands (project 15031) and industrial partners Bronkhorst, The Netherlands and KROHNE, The Netherlands.

Appendix. Derivation of the equation for the flow speed — linear and nonlinear version

In an in-line flow meter, the upstream and downstream transit times are:

$$t_{u} = \frac{D}{\sin \theta} \frac{1}{c_{0} - v_{m} \cos \theta},$$

$$t_{d} = \frac{D}{\sin \theta} \frac{1}{c_{0} + v_{m} \cos \theta}.$$
(A.1)

We can combine these expressions into:

$$\begin{aligned} \frac{1}{t_d} - \frac{1}{t_u} &= \frac{t_u - t_d}{t_u t_d} \\ &= \frac{\sin \theta}{D} (c_0 + v_m \cos \theta - c_0 + v_m \cos \theta) \\ &= 2 \sin \theta \cos \theta \frac{v_m}{D} \\ &= \sin 2\theta \frac{v_m}{D}, \end{aligned} \tag{A.2}$$

from which it follows that:

$$v_m = \frac{D}{\sin 2\theta} \frac{t_u - t_d}{t_u t_d} = \frac{D}{\sin 2\theta} \frac{\Delta t}{t_u t_d}.$$
 (A.3)

However, this does not yet give a linear relation between the flow speed v_m and the transit time difference Δt , because $t_u t_d$ still depends on v_m :

$$t_u t_d = \left(\frac{D}{\sin \theta}\right)^2 \frac{1}{(c_0 - v_m \cos \theta)(c_0 + v_m \cos \theta)}$$

$$= \left(\frac{D}{\sin \theta}\right)^2 \frac{1}{c_0^2 - v_m^2 \cos^2 \theta}.$$
(A.4)

A.1. Low flow speed

If $v_m \ll c_0$, we can neglect the $v_m^2 \cos^2 \theta$ term in the denominator of Eq. (A.4), and substitution into Eq. (A.3) then yields:

$$v_m = \frac{D}{\sin 2\theta} \left(\frac{\sin \theta}{D}\right)^2 c_0^2 \Delta t = \frac{c_0^2 \tan \theta}{2D} \Delta t, \tag{A.5}$$

which is the linear relation between v_m and Δt given in Eq. (2) of the main text.

A.2. Large flow speed

If $v_m \ll c_0$ no longer holds, we can directly substitute Eq. (A.4) into Eq. (A.3) and obtain:

$$v_m = \frac{D}{\sin 2\theta} \left(\frac{\sin \theta}{D}\right)^2 \Delta t (c_0^2 - v_m^2 \cos^2 \theta)$$

= $\frac{\tan \theta}{2D} \Delta t (c_0^2 - v_m^2 \cos^2 \theta)$. (A.6)

The inverse of this relation is:

$$\Delta t = \frac{2D}{\tan \theta} \frac{v_m}{c_0^2 - v_m^2 \cos^2 \theta}.$$
 (A.7)

Eqs. (A.6) and (A.7) are nonlinear relationships between v_m and Δt . The solutions for v_m are:

$$v_m = A(-1 \pm \sqrt{1+B}),$$
 (A.8)

with:

$$A = \frac{2D}{\sin 2\theta \, 4t},\tag{A.9}$$

$$B = \left(\frac{c_0 \Delta t \sin \theta}{D}\right)^2. \tag{A.10}$$

For the physically valid solution, we have chosen the + sign in Eq. (A.8).

References

- J. Delsing, Ultrasonic gas flow meter with corrections for large dynamic metering range, Ultrasonics 27 (6) (1989) 349–356.
- [2] D. Zheng, H. Hou, T. Zhang, Research and realization of ultrasonic gas flow rate measurement based on ultrasonic exponential model, Ultrasonics 67 (2016) 112–119.
- [3] H. Zhou, T. Ji, R. Wang, X. Ge, X. Tang, S. Tang, Multipath ultrasonic gas flow-meter based on multiple reference waves, Ultrasonics 82 (2018) 145–152.
- [4] Z. Fan, W. Jiang, W.M. Wright, Non-contact ultrasonic gas flow metering using air-coupled leaky lamb waves, Ultrasonics 89 (2018) 74–83.
- [5] S.F. Mousavi, S.H. Hashemabadi, J. Jamali, Calculation of geometric flow profile correction factor for ultrasonic flow meter using semi-3d simulation technique, Ultrasonics 106 (2020) 106165.
- [6] R.C. Baker, Flow Measurement HandBook: Industrial Designs, Operating Principles, Performance, and Applications, Cambridge University Press, 2005.
- [7] J. Van Deventer, J. Delsing, Apparent transducer non-reciprocity in an ultrasonic flow meter, Ultrasonics 40 (1–8) (2002) 403–405.
- [8] D. Kurniadi, A. Trisnobudi, A multi-path ultrasonic transit time flow meter using a tomography method for gas flow velocity profile measurement, Part. Part. Syst. Charact. 23 (3–4) (2006) 330–338.
- [9] S. Jacobson, P. Denbigh, D. Naude, A new method for the demodulation of ultrasonic signals for cross-correlation flowmeters, Ultrasonics 23 (3) (1985) 128–132.
- [10] A. Worch, A clamp-on ultrasonic cross correlation flow meter for one-phase flow, Meas. Sci. Technol. 9 (4) (1998) 622.
- [11] V. Skwarek, V. Hans, Multipath cross-correlation flowmeters, in: Proceedings of IMEKO, 2000, pp. 1–6.

J. Massaad et al. Ultrasonics 116 (2021) 106476

- [12] V. Skwarek, H. Windorfer, V. Hans, Measuring pulsating flow with ultrasound, Measurement 29 (3) (2001) 225–236.
- [13] P. Brassier, B. Hosten, F. Vulovic, High-frequency transducers and correlation method to enhance ultrasonic gas flow metering, Flow Meas. Instrum. 12 (3) (2001) 201–211.
- [14] E. Mandard, D. Kouame, R. Battault, J.-P. Remenieras, F. Patat, Methodology for developing a high-precision ultrasound flow meter and fluid velocity profile reconstruction, IEEE Trans. Ultrason. Ferroelectr. Freq. Control 55 (1) (2008) 161–172.
- [15] M.F. Hamilton, D.T. Blackstock, et al., Nonlinear Acoustics, Vol. 237, Academic Press, San Diego, 1998.
- [16] S. Brauers, Ultrasonic flow meters liquids, 2012, KROHNE Academy Online.
- [17] I. o'Sullivan, W. Wright, Ultrasonic measurement of gas flow using electrostatic transducers, Ultrasonics 40 (1–8) (2002) 407–411.
- [18] Q. Chen, W. Li, J. Wu, Realization of a multipath ultrasonic gas flowmeter based on transit-time technique, Ultrasonics 54 (1) (2014) 285–290.
- [19] Y.-S. Lee, M.F. Hamilton, Time-domain modeling of pulsed finite-amplitude sound beams, J. Acoust. Soc. Am. 97 (2) (1995) 906–917.
- [20] R.O. Cleveland, M.F. Hamilton, D.T. Blackstock, Time-domain modeling of finite-amplitude sound in relaxing fluids, J. Acoust. Soc. Am. 99 (6) (1996) 3312–3318.

- [21] X. Yang, R.O. Cleveland, Time domain simulation of nonlinear acoustic beams generated by rectangular pistons with application to harmonic imaging, J. Acoust. Soc. Am. 117 (1) (2005) 113–123.
- [22] M.M. Voormolen, 3D harmonic echocardiography, 2007.
- [23] J. Huijssen, Modeling of nonlinear medical diagnostic ultrasound, 2008.
- [24] A.C. Baker, A.M. Berg, A. Sahin, J.N. Tjøtta, The nonlinear pressure field of plane, rectangular apertures: Experimental and theoretical results, J. Acoust. Soc. Am. 97 (6) (1995) 3510–3517.
- [25] L. Svilainis, P. Kabisius, A. Aleksandrovas, A. Chaziachmetovas, Excitation signal's influence on ultrasonic transit time flow meter's performance, in: IOP Conference Series: Materials Science and Engineering, Vol. 42, IOP Publishing, 2012, 012047.
- [26] T. Folkestad, K.S. Mylvaganam, Chirp excitation of ultrasonic probes and algorithm for filtering transit times in high-rangeability gas flow metering, IEEE Trans. Ultrason. Ferroelectr. Freq. Control 40 (3) (1993) 193–215.
- [27] K. Mylvaganam, High-rangeability ultrasonic gas flowmeter for monitoring flare gas, IEEE Trans. Ultrason. Ferroelectr. Freq. Control 36 (2) (1989) 144–149.
- [28] W.-J. Zhu, K.-J. Xu, M. Fang, W. Wang, Z.-W. Shen, Mathematical modeling of ultrasonic gas flow meter based on experimental data in three steps, IEEE Trans. Instrum. Meas. 65 (8) (2016) 1726–1738.